# Family of Carboxylate- and Nitrate-diphenoxo Triply Bridged Dinuclear Ni(II)Ln(III) Complexes (Ln = Eu, Gd, Tb, Ho, Er, Y): Synthesis, Experimental and Theoretical Magneto-Structur...

**ARTICLE** *in* INORGANIC CHEMISTRY · MAY 2012

Impact Factor: 4.76 · DOI: 10.1021/ic3004596 · Source: PubMed



**8 AUTHORS**, INCLUDING:

Jose Ruiz
University of the Andes (Venezuela)
**54** PUBLICATIONS **1,076** CITATIONS
SEE PROFILE

Antonio J. Mota
University of Granada
**88** PUBLICATIONS **1,178** CITATIONS
SEE PROFILE

Eduard Cremades
University of Barcelona
**22** PUBLICATIONS **1,486** CITATIONS
SEE PROFILE

Eliseo Ruiz
University of Barcelona
**205** PUBLICATIONS **8,127** CITATIONS
SEE PROFILE

Inorganic Chemistry

Article

pubs.acs.org/IC

# Family of Carboxylate- and Nitrate-diphenoxo Triply Bridged Dinuclear $Ni^{II}Ln^{III}$ Complexes (Ln = Eu, Gd, Tb, Ho, Er, Y): Synthesis, Experimental and Theoretical Magneto-Structural Studies, and Single-Molecule Magnet Behavior

Enrique Colacio,*[,†] José Ruiz,[†] Antonio J. Mota,[†] María A. Palacios,[†] Eduard Cremades,[‡] Eliseo Ruiz,[‡] Fraser J. White,[§] and Euan K. Brechin*[,§]

[†]Departamento de Química Inorgánica, Facultad de Ciencias, Universidad de Granada, Av. Fuentenueva S/N, 18071 Granada, Spain

[‡]Departament de Química Inorgánica, Facultat de Química, Universitat de Barcelona, Martí i Franquès 1, 08028 Barcelona, Spain

[§]EaStCHEM School of Chemistry, The University of Edinburgh, West Mains Road, Edinburgh EH9 3JJ, United Kingdom

Supporting Information

**ABSTRACT:** Seven acetate-diphenoxo triply bridged $M^{II}$-$Ln^{III}$ complexes ($M^{II}$ = $Ni^{II}$ and $Ln^{III}$ = Gd, Tb, Ho, Er, and Y; $M^{II}$ = $Zn^{II}$ and $Ln^{III}$ = $Ho^{III}$ and $Er^{III}$) of formula $[M(\mu\text{-L})(\mu\text{-OAc})Ln(NO_3)_2]$, one nitrate-diphenoxo triply bridged $Ni^{II}$–$Tb^{III}$ complex, $[Ni(\mu\text{-L})(\mu\text{-NO}_3)Tb(NO_3)_2]\cdot 2CH_3OH$, and two diphenoxo doubly bridged $Ni^{II}$-$Ln^{III}$ complexes ($Ln^{III}$ = Eu, Gd) of formula $[Ni(H_2O)(\mu\text{-L})Ln(NO_3)_3]\cdot 2CH_3OH$ have been prepared in one pot reaction from the compartmental ligand *N*,*N*′,*N*″-trimethyl-*N*,*N*″-bis(2-hydroxy-3-methoxy-5-methylbenzyl)diethylenetriamine ($H_2L$). Moreover, $Ni^{II}$-$Ln^{III}$ complexes bearing benzoate or 9-anthracenecarboxylate bridging groups of formula $[Ni(\mu\text{-L})(\mu\text{-BzO})Dy(NO_3)_2]$ and $[Ni(\mu\text{-L})(\mu\text{-9-An})Dy(9\text{-An})(NO_3)_2]\cdot 3CH_3CN$ have also been successfully synthesized. In acetate-diphenoxo triply bridged complexes, the acetate bridging group forces the structure to be folded with an average hinge angle in the $M(\mu\text{-O}_2)Ln$ bridging fragment of ~22°, whereas nitrate-diphenoxo doubly bridged complexes and diphenoxo-doubly bridged complexes exhibit more planar structures with hinge angles of ~13° and ~2°, respectively. All $Ni^{II}$-$Ln^{III}$ complexes exhibit ferromagnetic interactions between $Ni^{II}$ and $Ln^{III}$ ions and, in the case of the $Gd^{III}$ complexes, the $J_{NiGd}$ coupling increases weakly but significantly with the planarity of the M–$(O)_2$–Gd bridging fragment and with the increase of the Ni–O–Gd angle. Density functional theory (DFT) theoretical calculations on the $Ni^{II}Gd^{III}$ complexes and model compounds support these magneto-structural correlations as well as the experimental $J_{NiGd}$ values, which were found to be ~1.38 and ~2.1 $cm^{-1}$ for the folded $[Ni(\mu\text{-L})(\mu\text{-OAc})Gd(NO_3)_2]$ and planar $[Ni(H_2O)(\mu\text{-L})Gd(NO_3)_3]\cdot 2CH_3OH$ complexes, respectively. The $Ni^{II}Dy^{III}$ complexes exhibit slow relaxation of the magnetization with $\Delta/k_B$ energy barriers under 1000 Oe applied magnetic fields of 9.2 and 10.1 K for $[Ni(\mu\text{-L})(\mu\text{-BzO})Dy(NO_3)_2]$ and $[Ni(\mu\text{-L})(\mu\text{-9-An})Dy(9\text{-An})(NO_3)_2]\cdot 3CH_3CN$, respectively.

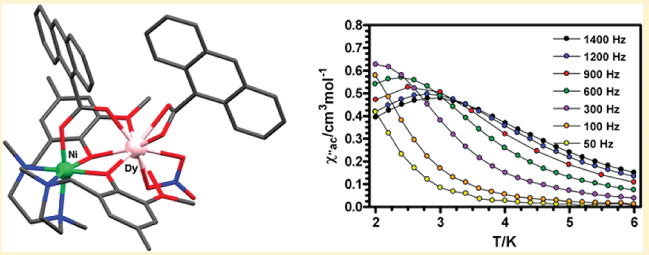


## INTRODUCTION

In recent years, heteropolynuclear 3d-4f complexes have been extensively studied not only because there exists a great interest in understanding the most important factors that govern the magnitude and nature of the magnetic exchange interaction between 3d and 4f metal ions but also because some 3d/4f metal aggregates behave as single-molecule magnets (SMMs).[1] These chemically and physically fascinating nanomagnets exhibit slow relaxation of the magnetization and magnetic hysteresis below the so-called blocking temperature ($T_B$) without undergoing long-range magnetic ordering[2] and therefore are potential candidates for magnetic data storage and for processing magnetic information at the molecular level.[3] The SMM behavior is due to the existence of an energy barrier that prevents reversal of the molecular magnetization and causes slow relaxation of the magnetization at low temperature. This energy barrier depends on the large-spin multiplicity of the ground state ($S_T$) and the easy-axis (or Ising-type) magnetic anisotropy of the entire molecule ($D < 0$). Nevertheless, recently, it has been shown that low-coordinate, high-spin iron(II) and cobalt(II) complexes with large and positive $D$ values can also exhibit SMM behavior.[4] The incorporation of heavy lanthanide ions, such as $Tb^{III}$, $Dy^{III}$, $Ho^{III}$, and $Er^{III}$, in cluster complexes is a sensible strategy for designing SMMs because they have large angular and magnetic moments in the ground multiplet state as a consequence of strong spin–orbit coupling, and because these metal ions are assumed to possess a large Ising-type magnetic anisotropy,[1] which depends on the shape and nature of the electrostatic ligand field around the

Received: February 29, 2012
Published: May 7, 2012

   dx.doi.org/10.1021/ic3004596 | Inorg. Chem. 2012, 51, 5857–5868

lanthanide ion.[1,5] Moreover, the magnetic coupling of the heavy lanthanide ions with 3d transition metal ions is often ferromagnetic, which leads to ground states with even larger magnetic moments.[1] SMM behavior has been shown to occur not only in large 3d-4f metal clusters with different metal core topologies,[1,6] which play an important role in determining the molecular anisotropy,[6b] but also in small dinuclear complexes.[1,7] The majority of these latter systems were prepared by following the general route initially developed by Costes et al.,[8] which uses compartmental Schiff base ligands derived from the condensation of different amines and *o*-vanillin. These types have allowed the preparation of a large number of Cu-Ln dinuclear complexes exhibiting ferromagnetic interactions between $Cu^{II}$ and $Ln^{III}$ ions,[1] and, in some cases, SMM behavior.[7] However, analogous complexes containing other 3d metal ions, such as $Ni^{II}$, $Co^{II}$, $VO^{II}$, and $Fe^{II}$, are much more scarce.[9] These complexes seem to follow the same trend as Cu-Ln ones, and they exhibit ferromagnetic exchange coupling for lanthanides ions with electronic configurations $f^7$-$f^{11}$.

Although $Ni^{II}$ has a second order orbital angular momentum that can provide large negative zero field splitting parameters, only a few examples of Ni-Ln dinuclear complexes with Schiff base compartmental ligands have been reported so far.[9h−n] Among them, the Dy-containing complexes have been shown to exhibit SMM properties.[9l−n] These Ni-Ln complexes have been less studied than the Cu-Ln examples, probably because there is no strict control over the coordination geometry of the 3d metal ion. Indeed in some cases Ni-Ln complexes containing diamagnetic square-planar Ni(II) ions were obtained.[10] To avoid this, we recently prepared a new and flexible non-Schiff base compartmental ligand ($H_2L$ = *N*,*N*′,*N*″-trimethyl-*N*,*N*″-bis(2-hydroxy-3-methoxy-5-methylbenzyl)diethylenetriamine, see Scheme 1) with a $N_3O_2$ pentacoordinated inner site that

**Scheme 1. Structure of the Ligand $H_2L$**

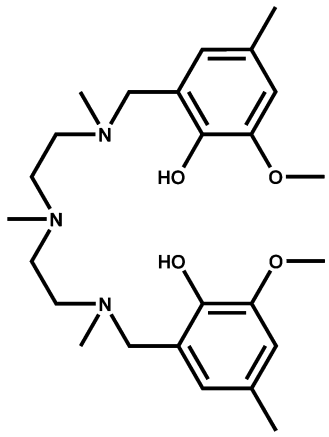


forces the $Ni^{II}$ ion to saturate its coordination sphere with a donor atom, leading to an octahedral, paramagnetic Ni(II) species. If the donor atom belongs to a bridging ligand connecting the 3d and 4f metal ions, triply bridged 3d-4f complexes can be obtained. In fact, we were able to prepare the first two examples of $Ni^{II}$−$Dy^{III}$ complexes containing triple diphenoxonitrate and diphenoxoacetate bridges, which exhibited SMM behavior.[9m] In this paper we report the synthesis, structural characterization, and magnetic properties of a series of doubly and triply bridged $Ni^{II}$-Ln dinuclear complexes ($Ln^{III}$ = Eu, Gd, Tb, Dy, Ho, Er, and Y) with the $H_2L$ ligand. This study aims to (i) confirm that the magnetic exchange interaction in the $Ni^{II}$-$Ln^{III}$ (Ln = Gd, Tb, Dy, Ho, Er) complexes is in all cases ferromagnetic in nature; (ii) investigate how the ferromagnetic exchange coupling varies with the folding of the $Ni(O)_2Ln$ bridging fragment and with the average Ln−O−Ni bridging angle, employing DFT theoretical calculations on the Ni−Gd complexes and model compounds; (iii) examine whether other diphenoxonitrate and diphenoxocarboxylate bridged $Ni^{II}$-Ln complex show SMM properties; (iv) modify the electric ligand field surrounding the Dy metal ion by changing either the bridging ligand or some of the ligands coordinated to the Dy ion, in an attempt to improve SMM properties

## EXPERIMENTAL SECTION

**General Procedures.** Unless stated otherwise, all reactions were conducted in oven-dried glassware in aerobic conditions, with the reagents purchased commercially and used without further purification. The ligand $H_2L$ was prepared as previously described.[9m]

**Preparation of Complexes. [Ni(μ-L)(μ-OAc)Ln(NO$_3$)$_2$] ($Ln^{III}$ = Gd (1), Tb (2), Ho (3), Er (4), Y (1a).** A general procedure was used for the preparation of these complexes: To a solution of $H_2L$ (56 mg, 0.125 mmol) in 5 mL of MeOH were subsequently added with continuous stirring 31.1 mg (0.125 mmol) of $Ni(OAc)_2{\cdot}4H_2O$ and 0.125 mmol of $Ln(NO_3)_3{\cdot}nH_2O$. The resulting pale green solution was filtered and allowed to stand at room temperature. After one day, well formed prismatic light blue crystals of compounds **1**−**4** were obtained with yields in the range 60−65% based on Ni.

**[Zn(μ-L)(μ-OAc)Ln(NO$_3$)$_2$] ($Ln^{III}$ = Ho (5), Er (6)).** These compounds were prepared in a 60% yield as colorless crystals following the same procedure as for **1**−**4**, but using $Zn(OAc)_2{\cdot}2H_2O$ (27 mg, 0.125 mmol) instead of $Ni(OAc)_2{\cdot}4H_2O$.

**[Ni(μ-L)(μ-NO$_3$)Tb(NO$_3$)$_2$]·2CH$_3$OH (7) and [Ni(H$_2$O)(μ-L)Ln(NO$_3$)$_3$]·2CH$_3$OH ($Ln^{III}$ = Eu (8a) and Gd (8)).** These compounds were prepared in a 60% yield as light blue crystals following the procedure for **1**−**4**, except that $Ni(NO_3)_2{\cdot}6H_2O$ (36 mg, 0.125 mmol) was used instead of $Ni(OAc)_2{\cdot}4H_2O$.

**[Ni(μ-L)(μ-OBz)Dy(NO$_3$)$_2$]·CH$_3$OH (9) (OBz = benzoate).** To a solution of $H_2L$ (56 mg, 0.125 mmol) in 5 mL of MeOH were subsequently added 36 mg (0.125 mmol) of $Ni(NO_3)_2{\cdot}6H_2O$ and 46 mg (0.125 mmol) of $Dy(NO_3)_3{\cdot}5H_2O$ with continuous stirring. The light blue solution was filtered, and then 19 mg (0.125 mmol) of NaOBz were added with continuous stirring. After two days the filtered solution afforded light blue crystals in a 60% yield.

**[Ni(μ-L)(μ-9-An)Dy(9-An)(NO$_3$)$_2$]·3CH$_3$CN (10) (9-An = 9-antharecenecarboxylate).** To a solution of $H_2L$ (56 mg, 0.125 mmol) in 5 mL of MeOH were subsequently added 36 mg (0.125 mmol) of $Ni(NO_3)_2{\cdot}6H_2O$ and 46 mg (0.125 mmol) of $Dy(NO_3)_3{\cdot}5H_2O$ with continuous stirring. To this solution was added dropwise another solution containing 28 mg of 9-anthracenecarboxylic acid (0.125 mmol) and 0.125 mmol of triethylamine, immediately affording a green precipitate, which filtered off and recrystallized from acetonitrile. The resulting solution was filtered, eliminating any amount of insoluble material, and allowed to stand at room temperature for two days, whereupon crystals of **10** were formed in a yield of 45%.

The purity of the complexes was checked by elemental analysis (see Supporting Information, Table S1).

**Physical Measurements.** Elemental analyses were carried out at the "Centro de Instrumentación Científica" (University of Granada) on a Fisons-Carlo Erba analyzer model EA 1108. IR spectra on powdered samples were recorded with a ThermoNicolet IR200FTIR using KBr pellets. Magnetization and variable temperature (2−300 K) magnetic susceptibility measurements on polycrystalline samples were carried out with a Quantum Design SQUID MPMS XL-5 device operating at different magnetic fields. The experimental susceptibilities were corrected for the diamagnetism of the constituent atoms using Pascal's tables.


dx.doi.org/10.1021/ic3004596 | *Inorg. Chem.* 2012, 51, 5857−5868

**Single-Crystal Structure Determination.** Suitable crystals of **1**–**10** were mounted on a glass fiber and used for data collection. For compounds **1**, **2**, **7**, and **9**, data were collected with a dual source Oxford Diffraction SuperNova diffractometer equipped with an Atlas CCD detector and an Oxford Cryosystems low temperature device operating at 100 K and using Mo-$K_\alpha$. Semiempirical (multiscan) absorption corrections were applied using Crysalis Pro.[11] For compounds **1a**, **3**, **4**, **5**, **6**, **8**, **8a**, and **10** data were collected with a Bruker AXS APEX CCD area detector equipped with graphite monochromated Mo K$\alpha$ radiation ($\lambda$ = 0.71073 Å) by applying the $\omega$-scan method. Lorentz-polarization and empirical absorption corrections were applied. The structures were solved by direct methods and refined with full-matrix least-squares calculations on $F^2$ using the program SHELXS97.[12] Anisotropic temperature factors were assigned to all atoms except for the hydrogens, which are riding their parent atoms with an isotropic temperature factor arbitrarily chosen as 1.2 times that of the respective parent. Final $R(F)$, $wR(F^2)$, and goodness of fit agreement factors, details on the data collection and analysis can be found in Supporting Information, Tables S2 and S3. Selected bond lengths and angles are given in Supporting Information, Tables S4 and S5.

**Computational Details.** DFT calculations were performed using the SIESTA (Spanish Initiative for Electronic Simulations with Thousands of Atoms) code[13] together with the PBE functional.[14] Only valence electrons are included in the calculations, with the core being replaced by norm-conserving scalar relativistic pseudopotentials factorized in the Kleinman-Bylander form.[15] The pseudopotentials are generated according to the procedure of Trouiller and Martins.[16] For gadolinium atoms, we used the pseudopotential and triple-$\zeta$ basis set proposed by Pollet et al.[17] We also have employed a numerical basis set of triple-$\zeta$ quality functions for the nickel atoms and a double-$\zeta$ one with polarization functions for the main group elements. In the calculations, values of 50 meV for the energy shift and 250 Ry for the mesh cutoff have been employed because they provide a good compromise between accuracy and computer time to estimate exchange coupling constants

To calculate the exchange coupling constant ($J$) a high-spin state (both gadolinium and nickel spins are parallely aligned, hence $S = 9/2$) and a low-spin solution (nickel spin is antiparallely aligned to gadolinium spin, $S = 5/2$) has been computed. For GGA functionals, such as the PBE expression used in our calculations, the broken-symmetry approximation (without spin-projection) has been employed[18−20] to calculate the $J$ value through the following equation:

$$J = \frac{E_{LS} - E_{HS}}{2S_1S_2 + S_2}$$

where $S_1$ and $S_2$ are the local spins on centers 1 and 2, respectively, and $S_1 > S_2$. Thus, in the case of the $Ni^{II}Gd^{III}$ complexes it becomes:

$$J = \frac{E_{S=5/2} - E_{S=9/2}}{8}$$

## RESULTS AND DISCUSSION

The reaction of $H_2L$ with either $Ni(OAc)_2{\cdot}4H_2O$ or $Zn(OAc)_2{\cdot}2H_2O$ and subsequently with $Ln(NO_3)_3{\cdot}nH_2O$ in MeOH in 1:1:1 molar ratio led to light blue crystals of the compounds $[Ni(\mu\text{-}L)(\mu\text{-}OAc)Ln(NO_3)_2]$ ($Ln^{III}$ = Gd (**1**), Tb (**2**), Ho (**3**), Er (**4**), and Y (**1a**)) and colorless crystals of the compounds $[Zn(\mu\text{-}L)(\mu\text{-}OAc)Ln(NO_3)_2]$ ($Ln^{III}$ = Ho (**5**) and Er(**6**)), respectively. The same reaction but using $Ni(NO_3)_3{\cdot}6H_2O$ instead of $Ni(OAc)_2{\cdot}4H_2O$ and $Ln(NO_3)_3{\cdot}6H_2O$ ($Ln^{III}$ = Eu, Gd, Tb) led to two different Ni-Ln dinuclear complexes $[Ni(\mu\text{-}L)(\mu\text{-}NO_3)Tb(NO_3)_2]{\cdot}2CH_3OH$ (**7**) and $[Ni(H_2O)(\mu\text{-}L)Ln(NO_3)_3]{\cdot}2CH_3OH$ and ($Ln^{III}$ = Gd (**8**) and Eu (**8a**)). Ni-Ln complexes, bearing carboxylate bridging groups other than acetate, could be prepared by reacting a methanolic solution containing $H_2L$, $Ni(NO_3)_3{\cdot}6H_2O$, and $Dy(NO_3)_3{\cdot}6H_2O$ in 1:1:1 molar ratio with either NaOBz or a 9-anthracene carboxylic/$Et_3N$ mixture in 1:1 molar ratio. Following this route, the complexes $[Ni(\mu\text{-}L)(\mu\text{-}BzO)Dy(NO_3)_2]$ (**9**) and $[Ni(\mu\text{-}L)(\mu\text{-}9\text{-}An)Dy(9\text{-}An)(NO_3)_2]{\cdot}3CH_3CN$ (**10**) were successfully obtained in good yield. As expected, compound **9** has a benzoate bridging group connecting $Ni^{II}$ and $Dy^{III}$ ions, whereas, surprisingly, compound **10** has both bridging and chelate bidentate 9-anthracenecarboxylate ligands, the latter coordinated to the $Dy^{III}$ ion. We do not know at this stage why compound **10** is formed when a Ni–Dy/9-An = 1:1 molar ratio is used.

The diffuse reflectance electronic spectra of these complexes in the visible region show two absorption bands around 16100 $cm^{-1}$ and 9300 $cm^{-1}$ and one sharp and weak peak around 12500 $cm^{-1}$ (the electronic spectra of compound **8** is given as an example in Supporting Information, Figure S1). The two former are due to the $^3A_{2g} \rightarrow {}^3T_{1g}$ (F) and $^3A_{2g} \rightarrow {}^3T_{2g}$ transitions, whereas the peak on the high energy side of the lowest energy spin-allowed band is due to the spin-flip forbidden transition $^3A_{2g} \rightarrow {}^1E_g$ that gains intensity from the allowed $^3A_{2g} \rightarrow {}^3T_{2g}$ transition (stolen intensity).[21] Deviations from octahedral symmetry caused by the mixed ligand $NiN_3O_3$ coordination spheres do not lead to multiple band maxima for any of the spin allowed bands. A formal reason for this is the high holohedrized symmetry of the ligand-field potential in these complexes.[22] The holohedrized symmetry, obtained for orthoaxial complexes by replacing individual ligands along one axis by their average ligand-field strength is almost $O_h$ with very similar total ligand field strengths along the three axes, indicating that any splitting of the $^3T_{2g}$ and $^3T_{1g}$ states for octahedral symmetry should be small. Nevertheless, the $^3T_{2g}$ absorption band is particularly broad with a width at half height of 3000 $cm^{-1}$, which might be due to the strong trigonal distortion of the $NiN_3O_3$ coordination sphere of these complexes leading to multiple close maxima that give rise to the envelope of the band. The crystal field splitting, 10 Dq, that corresponds with the low energy band maximum, is higher than that observed for homoleptic complexes with oxygen ligator atoms, such as $[Ni(H_2O)]^{2+}$, and lower than that found for strong-field complexes such as $[Ni(o\text{-phenanthroline})_3]^{2+}$.[22] It is interesting to note that the fact that all complexes exhibit virtually identical visible spectra is a clear indication of the almost identical geometry of the $Ni^{II}$ coordination sphere in these complexes (see below). As expected for the low absorption coefficient of the lanthanide bands (f-f transitions are strictly parity forbidden), no f-f absorption bands could be detected in the electronic spectra of the $Ni^{II}$-$Ln^{III}$ complexes.

**Crystal Structures.** Complexes **1**–**4** are isostructural between them and to the Ni–Dy and Zn–Dy analogues previously reported by us[9m] and crystallize in the triclinic $P\bar{1}$ space group. The structure of **1** is given as an example in Figure 1.

The structure consists of two almost identical dinuclear $M^{II}$-$Ln^{III}$ molecules, in which the $Ln^{III}$ and $Ni^{II}$ ions are bridged by two phenoxo groups of the $L^{2-}$ ligand and one *syn-syn* acetate anion. Compound **5** in the monoclinic $P21/n$ space group and its structure is very similar to those of **1**–**4** but having only one crystallographically independent $Zn^{II}$-$Ln^{III}$ molecule.

In all these complexes, the $M^{II}$ ion ($Zn^{II}$ and $Ni^{II}$) exhibits a slightly trigonally distorted $NiN_3O_3$ coordination polyhedron, where the three nitrogen atoms from the amine groups, and consequently the three oxygen atoms belonging to the acetate and phenoxo bridging groups, occupy *fac* positions. The


dx.doi.org/10.1021/ic3004596 | Inorg. Chem. 2012, 51, 5857–5868

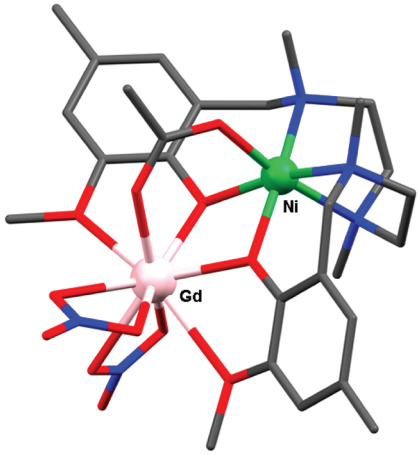


**Figure 1.** Perspective view of one of the crystallographic independent molecules of complex **1**. Color code: N = blue, O = red, Ni = green, Dy = pink, C = gray.

calculation of the degree of distortion of the Ni(II) coordination polyhedron with respect to ideal six-vertex polyhedra, by using the continuous shape measure theory and SHAPE software,[23] indicates that the $NiN_3O_3$ coordination spheres are found in the OC-6 ↔ TPR-6 deformation pathway (deviating by less than 10% from this pathway) and are close to the octahedral geometry (∼72%) somewhat distorted to trigonal prismatic (Supporting Information, Table S6). The $ZnN_3O_3$ coordination sphere is even more distorted with a 59.5% of octahedral geometry. The average Ni−O and Ni−N distances are very similar and range from 2.041(2) Å to 2.144(3) Å and from 2.131(3) Å to 2.183(2) Å, respectively. The Zn−O and Zn−N distances are found in the ranges 2.033(3)Å to 2.187(2) Å and from 2.195(4) Å to 2.257(3) Å, respectively. In all complexes, the corresponding $Ln^{III}$ ion exhibits a $LnO_9$ coordination sphere, consisting of the two phenoxo bridging oxygen atoms, the two methoxy oxygen atoms, one oxygen atom from the acetate bridging group, and four oxygen atoms belonging to two bidentate nitrate anions. The $LnO_9$ coordination sphere is rather asymmetric, exhibiting short $Ln-O_{phenoxo}$ and $Ln-O_{acetate}$ bond distances in the range 2.2−2.4 Å and longer $Ln-O_{nitrate}$ and $Ln-O_{methoxy}$ bond distances >2.4 Å (one of the methoxy groups is weakly coordinated with Ln−O bond distances >2.6 Å). In fact, the use of the continuous shape measure theory and SHAPE software, indicates that the $LnO_9$ coordination sphere can be considered as intermediate between several nine-vertex polyhedra (Supporting Information, Table S7).

As expected, the average $Ln-O_{phenoxo}$ bond distances for compounds **1**−**4**, and the isostructural Ni−Dy complex,[9m] steadily decrease from $Gd^{III}$ to $Er^{III}$ following the lanthanide contraction, with a concomitant decrease of the average Ni-Ln and $Ln-O_{acetate}$ bond distances. In fact, these bond distances show a linear dependence with the $Ln^{III}$ ionic radii (Figure 2) with correlation coefficients $r^2$ >0.99 and almost the same slope. Although the Ni−O−Ln bridging angles follow the same trend, they are less sensitive to the effect of the lanthanide contraction.

The Ni(di-$\mu$-phenoxo)($\mu$-acetate)Ln bridging fragment is rather asymmetric, not only because the $Ln-O_{phenoxo}$ and $Ni-O_{phenoxo}$ bond distances are different but also because there exist two different Ni−O−Ln bridging angles with average values of 107.20° and 101.25° for complexes **1**−**4**.

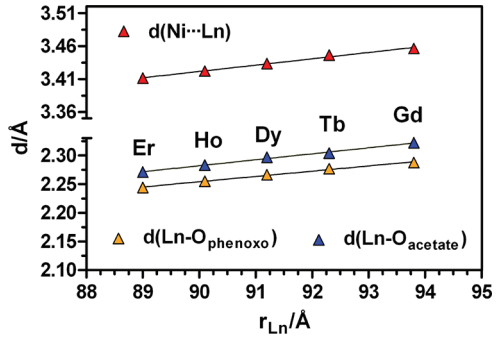


**Figure 2.** Plots of the Ni···Ln, $Ln\cdots O_{phenoxo}$, and $Ln-O_{acetate}$ versus the $Ln^{III}$ ionic radius.

The bridging acetate group forces the structure to be folded with the average hinge angle of the M($\mu$-$O_2$)Ln bridging fragment ranging from 21.4° for **1** to 22.0° for **4** (the hinge angle, $\beta$, is the dihedral angle between the O−Ni−O and O−Ln−O planes in the bridging fragment). Therefore, the hinge angle increases with the decrease of the $Ln^{III}$ size, as expected.

The Ni−Y complex (**1a**) is isostructural with complexes **1**−**4**, and the structural parameters for the Zn-Ln complex **5** are very similar to those observed for the analogous complex **4** and therefore their structures do not deserve further comment. It should be noted that all attempts to obtain suitable crystals for X-ray crystallography of compound **6** failed. Nevertheless, its IR spectrum and X-ray powder diffractogram clearly indicate that **5** and **6** are isostructural (Supporting Information, Figure S2)

As indicated above, the reaction of the $H_2L$ ligand with $Ni(NO_3)_3{\cdot}6H_2O$ and subsequently with $Tb(NO_3)_3{\cdot}6H_2O$ afforded light blue crystals of the compound [Ni($\mu$-L)($\mu$-$NO_3$)$Tb(NO_3)_2$]·$2CH_3OH$ (**7**), which is isostructural with the Ni−Dy analogue previously reported by us. Its molecular structure (Figure 3) is very similar to that of compounds **1**−**5** but having a bridging nitrate anion connecting the $Tb^{III}$ and $Ni^{II}$ metal ions instead of an acetate anion.

The coordination of the nitrato bridging ligand folds the Ni($\mu$-$O_2$)Tb bridging fragment of the structure but to a lesser extent than in compounds **1**−**5**. Thus, the hinge angle decreases to a value of approximately 13.7° with a concomitant decrease of the out-of-plane displacements of the O−C bonds

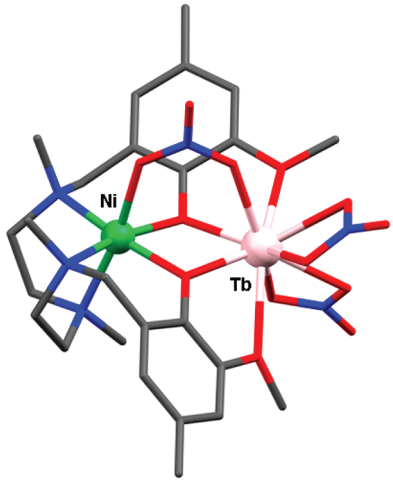


**Figure 3.** Perspective view of the molecular structure of **7**. Color code: N = blue, O = red, Ni = green, Dy = pink, C = gray.


dx.doi.org/10.1021/ic3004596 | Inorg. Chem. 2012, 51, 5857−5868

belonging to the phenoxo bridging groups from the $Ni(O)_2Ni$ plane. Bond distances are very similar to those of complexes **1**–**5** except for the Ni–O and Tb–O bond distances involving the oxygen atoms of the bridging anion, which increase on going from acetate to nitrate by approximately 0.05 Å and 0.1 Å, respectively. Notice that the computed shape measures relative to the ideal six-vertex and nine-vertex polyhedra, for the $NiN_3O_3$ and $TbO_9$ coordination polyhedra, respectively, were very close to those obtained for compounds **1**–**4** (Supporting Information, Table S6).

The reaction of the $H_2L$ ligand with $Ni(NO_3)_3{\cdot}6H_2O$ and subsequently with $Gd(NO_3)_3{\cdot}6H_2O$ does not lead to the diphenoxonitrate triply bridged $Ni^{II}$-$Gd^{III}$ complex but to the complex $[Ni(H_2O)(\mu\text{-}L)Ln(NO_3)_3]{\cdot}2CH_3OH$ (**8**), where the $Ni^{II}$ and $Gd^{III}$ metal ions are connected only by a double phenoxo bridge (Figure 4)

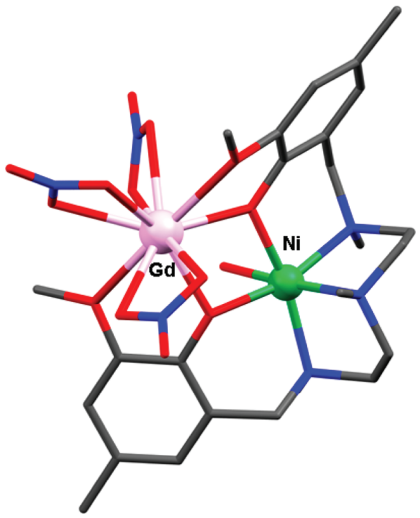


**Figure 4.** Perspective view of the molecular structure of **8**. Color code: N = blue, O = red, Ni = green, Dy = pink, C = gray.

The lack of a nitrate bridging group in **8** promotes the following important structural changes with regard to the structure of **7** (see Figure 5). (i) The $Ni(\mu\text{-}O_2)Gd$ bridging fragment becomes almost planar with a hinge angle of 2.3° and rather symmetric with Ni–O–Gd bridging angles of 109.70° and 109.25°. (ii) The preferred octahedral geometry for the $Ni^{II}$ ions is accomplished by the coordination of a water molecule, inducing a higher asymmetry on the Ni(II) coordination sphere (Supporting Information, Table S6). (iii) The coordination of one additional bidentate chelating nitrate ligand to the $Gd^{III}$ ion leads to an expanded $GdO_{10}$ coordination sphere and provokes a deformation in both the O···Gd bond distance and location of the coordinated methoxy groups, ultimately leading to a larger Ni···Gd separation.

It should be noted at this point that all attempts to obtain other di-$\mu$-phenoxo $Ni^{II}$-$Ln^{III}$ ($Ln^{III}$ = Tb, Dy, Ho, Er) dinuclear complexes analogous to **8** were unsuccessful, and always triply bridged diphenoxonitrate complexes were obtained. It seems that the $Ln^{III}$ size might play an important role in the adoption of the final structural type. Thus, the larger $Gd^{III}$ ion could originate a significant strain in the weakly bonded nitrate bridging ligand, so that the di-$\mu$-phenoxo-bridged planar structure would be more favorable than the diphenoxonitrate-bridged folded one. To theoretically and experimentally

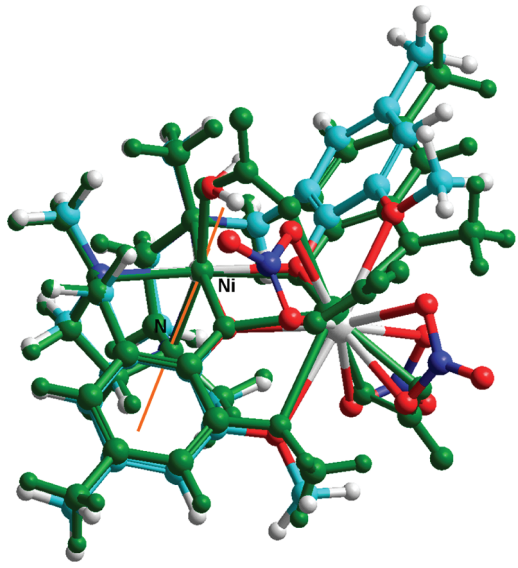


**Figure 5.** Simultaneous perspective of the optimized structures of complex **8** (N = blue, O = red, Ni = green, Dy = pink, C = gray) and the hypothetical nitrate bridged analogue (green) aligned along the Ni–N axis indicated in the figure, emphasizing the structural differences between them.

support this hypothesis we have performed DFT calculations on the optimized structures of compound **8** and the hypothetical nitrate-bridged complex $[Ni(\mu\text{-}L)(\mu\text{-}NO_3)Gd(NO_3)_2]$ which would be structurally analogous to complex **7** (Figure 5). Second, we have prepared the corresponding Ni-Ln dinuclear complex with $Eu^{III}$, which is larger in size than the $Gd^{III}$ analogue. In line with the experimental findings, DFT results confirm that the formation of **8** from $[Ni(\mu\text{-}L)(\mu\text{-}NO_3)Gd(NO_3)_2]$ would be a spontaneous process with $\Delta E$ = −15.3 kcal mol$^{-1}$, $\Delta H$ = −13.1 kcal mol$^{-1}$, and $\Delta G$ = −1.3 kcal mol$^{-1}$. In addition to this, the X-ray crystal structure of $[Ni(H_2O)(\mu\text{-}L)Eu(NO_3)_3]{\cdot}2CH_3OH$ (**8a**), which is isostructural with compound **8**, seems to support the $Ln^{III}$ size-structure dependence of the complexes bearing three nitrate anions.

The structure of compound **9** (Figure 6) is very similar to that of the complex $[Ni(\mu\text{-}L)(\mu\text{-}OAc)Dy(NO_3)_2]$, but having a benzoate bridging ligand instead of an acetate ligand connecting the $Ni^{II}$ and $Dy^{III}$ ions.

Compared to the acetate bridged analogue, **9** exhibits a small hinge angle (20.6°) and smaller and closer Ni–O–Ln bridging

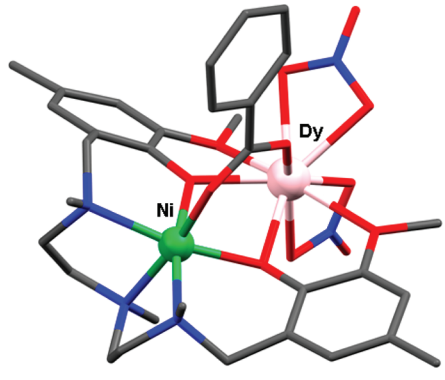


**Figure 6.** Perspective view of the molecular structure of **9**. Color code: N = blue, O = red, Ni = green, Dy = pink, C = gray.


dx.doi.org/10.1021/ic3004596 | *Inorg. Chem.* 2012, 51, 5857–5868

angles (102.1° and 105.6°), resulting in a lesser degree of asymmetry in the bridging region. The phenyl ring is almost coplanar with the carboxylate plane with a dihedral angle of 6.8°. Bond distances and angles in the remainder of the molecule are very close to those of the acetate bridged analogue.

The structure of **10** contains two 9-anthracene carboxylate bidentate ligands, one acting as a bridge linking the $Ni^{II}$ and $Dy^{III}$ ions and the other one acting as a chelating ligand coordinated to the $Dy^{III}$ ion (see Figure 7).

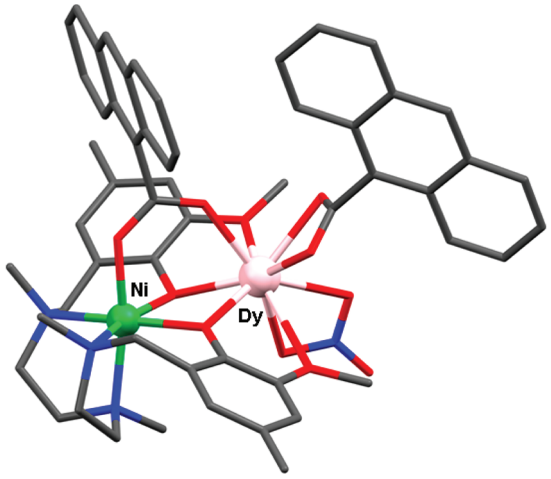


**Figure 7.** Perspective view of the molecular structure of **10**. Color code: N = blue, O = red, Ni = green, Dy = pink, C = gray.

It is interesting to note that **10** crystallizes in a non-centrosymmetric space group and therefore is chiral. Compound **10** represents a new example of a chiral molecule obtained from achiral starting materials. The overall ensemble of the crystals in a batch of **10** can be expected to contain crystals of both enantiomeric forms in equal amounts and therefore to be racemic. In addition to this, the most relevant differences between the structures of **9** and **10** are as follows: (i) the plane of the anthracene rings are not coplanar with the corresponding plane of carboxylate group, with dihedral angles between these planes of 88.2° and 83.4°, for the bridging and chelating 9-anthracene carboxylate ligands (9-An), respectively. The dihedral angle between the planes of the anthracene rings for the two 9-An ligands being 56°. (ii) The Dy–O bond distances involving the oxygen atoms of the chelating 9-anthracene carboxylato of ~2.4 Å are shorter than the Dy–$O_{nitrate}$ ones of ~2.5 Å and are located at the opposite site of the phenoxo oxygen atoms, which exhibit the shortest Ln–O distance on the $DyO_9$ coordination sphere. This leads to rather asymmetric ligand field around the $Dy^{III}$ ion.

Complexes **9** and **10** exhibit shape measure coefficients for the Ni(II) and Ln(III) atoms similar to those found for complexes **1**–**5**.

Finally, it should be stressed that only compounds **8** and **9** exhibit hydrogen bond interactions. In the case of **8**, these interactions are both intermolecular and intramolecular in nature. The former involve the molecules of methanol, the coordinated water molecule, and one of the nitrate anions belonging to two centrosymmetrically related $Ni^{II}$-$Gd^{III}$ molecules with donor-acceptor distances in the range 2.599–2.792 Å (Supporting Information, Figure S3). The latter involve the water molecule and one of the nitrate anions of the same $Ni^{II}$-$Gd^{III}$ with O···O distances of 2.918 Å. In the case of **9**, there exists only a hydrogen bond between the oxygen atom of one of the coordinated nitrate anions and the molecule of methanol with a donor-aceptor distance of 2.927 Å.

**Magnetic Properties.** The magnetic properties of the dinuclear complexes **1**–**10** were measured on polycrystalline samples in the 2–300 K temperature range under an applied magnetic field of 0.1 T. The data for compounds **1**–**2** and **7**–**10** in the form $\chi_M T$ versus $T$ are shown in Figure 8, whereas those of compounds **3**–**6** are given in Figure 12.

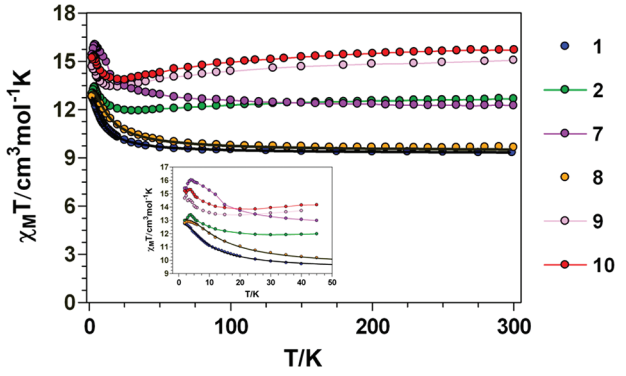


**Figure 8.** Temperature dependence of the $\chi_M T$ product at 1000 Oe for complexes **1**–**2** and **7**–**10**. Inset highlights the low temperature data. Black solid lines show the best fits for complexes **1** and **8**. The rest of the solid lines are a guide to the eye.

We start with the simpler cases concerning the Ni–Gd complexes **1** and **8**. The room temperature $\chi_M T$ values for **1** and **8** of 9.32 $cm^3$ K $mol^{-1}$ and 9.64 $cm^3$ K $mol^{-1}$, respectively, are slightly high but still in relative good agreement with the expected value for a couple of noninteracting $Ni^{II}$ ($S$ = 1) and $Gd^{III}$ ($S$ = 7/2) ions (8.875 $cm^3$ K $mol^{-1}$ with $g$ = 2). On lowering the temperature, the $\chi_M T$ slowly increases from room temperature to 50 K (9.62 $cm^3$ K $mol^{-1}$) for **1** and 60 K (9.98 $cm^3$ K $mol^{-1}$) for **8** and then in a more abrupt way to reach values of 12.75 $cm^3$ K $mol^{-1}$ at 2 K and 12.88 $cm^3$ K $mol^{-1}$ at 3 K, for **1** and **8**, respectively. This behavior is due to a ferromagnetic interaction between the $Ni^{II}$ and $Gd^{III}$ ions leading to a $S_T$ = 9/2 ground spin state. In the case of **8**, below 3 K, the $\chi_M T$ decreases to reach a value of 12.80 $cm^3$ K $mol^{-1}$at 2 K, which is probably associated to the zero-field splitting effect of the $Ni^{II}$ ion and/or weak antiferromagnetic interactions between dinuclear units mainly mediated by hydrogen bond interactions. The magnetic properties of these two compounds have been modeled by using the following Hamiltonian:

$$H = -JS_{Ni}S_{Gd} + D_{Ni}S_{Niz}{}^2 \qquad \text{(eq. 1)}$$

where $J$ accounts for the magnetic exchange coupling between $Ni^{II}$ and $Gd^{III}$ ions and $D_{Ni}$ accounts for the axial single ion zero-field splitting parameter of the $Ni^{II}$ ion. The fit of the experimental susceptibility data with the above Hamiltonian using the MAGPACK program[24] afforded the following set of parameters: $J$ = +1.38 $cm^{-1}$, $g$ = 2.04, $D$ = 2.5 $cm^{-1}$, and $R$ = 1.2 × $10^{-5}$ for **1**, and $J$ = +2.14 $cm^{-1}$, $g$ = 2.06, $D$ = 3.9 $cm^{-1}$, and $R$ = 2.1 × $10^{-5}$ for **8**. Compared to **1**, complex **8** exhibits a slightly higher value of the $D$ parameter, which is not unexpected in view of the higher trigonal distortion observed for the latter compound. The value of the $D_{Ni}$ parameter for the acetate


dx.doi.org/10.1021/ic3004596 | Inorg. Chem. 2012, 51, 5857–5868

**Table 1. Magneto-Structural Data for Alkoxo- and Phenoxo Polynuclear $Ni_xGd$ ($x$ =1, 2, 3) Complexes**

| complex | $J_{exp}$ ($cm^{-1}$) | $J_{calc}$ ($cm^{-1}$) | $\theta$ (deg)[a] | $\beta$ (deg)[a] | Gd···Ni (Å)[a] | ref. |
|---|---|---|---|---|---|---|
| $[Ni(H_2O)(\mu\text{-L})Ln(NO_3)_3]\cdot 2CH_3OH$ (**C-2**) (**8**) | +2.16 | +3.3 | 109.4 | 2.3 | 3.565 | T.w. |
| $[Ni_2Gd(L^1)_2(NO_3)_3(H_2O)_4]NO_3\cdot nH_2O$ (**O-2**) | +1.58 | | 108.9 | 4.45 | 3.691 | 25 |
| $[(L^2Ni(H_2O))_2Gd(H_2O)](CF_3SO_3)_3$ (**C-2**) | +4.8/0.05[b] | | 107.5 | 19.48 | 3.534 | 26 |
| $[L^2Ni(H_2O)_2Gd(NO_3)_3]$ (**C-2**) | +3.6 | +2.14 | 107.2 | 2.8 | 3.522 | 9h |
| $[Ni(CH_3CN)_2(valpan)Gd(NO_3)_3]\cdot CH_3CN$ (**C-2**) | +2.3 | | 106.1 | 0.22 | 3.467 | 9n |
| $[Ni(\mu\text{-L})(\mu\text{-Ac})Gd(NO_3)_2]$ (**C-2**) (**1**) | +1.38 | +2.05 | 104.4 | 21.4 | 3.456 | T.w. |
| $[(H_2O)Ni(ovan)_2(\mu\text{-}NO_3)Gd(ovan)(NO_3)_2]H_2O$ (**C-2**) | +1.36[c] | | 101.6 | 0.8 | 3.324 | 9k |
| $[Ni_2Gd\{(py)_2C(OEt)(O)\}_3\{(py)_2C(OH)(O)\}(NO_3)(H_2O)](ClO_4)_2$ (**O-2**) | +1.03 | | 101.5 | 16.3 | 3.427 | 27 |
| $[(L^3Ni)_2Gd](NO_3)$ (**T-3**) | +0.91 | | 95.6 | 49.1 | 3.323 | 28 |
| $[L^4 2Ni2Gd][ClO_4]$ (**T-3**) | +0.75 | | 95.0 | 49.5 | 3.314 | 29 |
| $[Ni_3Gd\{(py)_2C(H)O\}_6](ClO_4)_3$ (**O-2**) | −2,18 | | 94.8 | 1.06 | 3.203 | 30 |
| $[(NiL^5)Gd(hfac)_2(EtOH)]$ (**T-3**) | +0.34 | +0.36 | 91.3 | 51.3 | 3.210 | 9l |
| $[GdNiL^6(DMF)](ClO_4)_2\cdot CH_3CN$ (**M-3**) | +0.56 | | 90.8 | 52.0 | 3.169 | 9j |
| $[NiGd\{pyCO(OEt)pyC(OH)(OEt)py\}_3](ClO_4)_2$ (**O-3**) | −0.23 | | 85.7 | 58.3 | 2.987 | 31 |

[a]Average values. [b]There are two $J_{NiGd}$ as the $GdNi_2$ trinuclear complex is not centrosymmetric; [c]No available structural data and those included in the table correspond to the $YNi_2$ isostructural complex; $L^1$ = 2,6-di(acetoacetyl)pyridine; $L^2$ = *N*,*N*-2,2-dimethylpropylenedi(3-methoxysalicylideneiminato); valpan = *N*,*N*-propylenedi(3-methoxysalicylideneiminato); ovan =*o*-vanillin; $L^3$ = Schiff-base resulting from the 1: 3 condensation of trihydrochloride of triamine- 1,1,1-tris(aminomethyl)ethane with o-vanillin; $(py)_2C(H)O$ = di-2-pirydylketone $L^4$ = (S)P[N(Me)*N* = CH-$C_6H_3$-2-O-3-OMe]$_3$); $L^5$ = 1,1,1-tris(*N*-salicylideneaminomethyl)ethane; $L^6$ = Macrocyclic Schiff-base resulting from the 1: 1 condensation of tris(2-aminoethyl)amine with 2,6-diformyl-4-dichlorophenol; pyCOpyC(OH)py = di-2,6-(2-pyridylcarbonyl)pyridine; C-2 = compartmental ligand with two phenoxo bridging groups; T-3 = tripodal ligand with three phenoxo-bridging groups. M-3 = macrocyclic ligand with three phenoxo-bridging groups. O = open alkoxo-bridging ligands. T.w. = This work. $\theta$ is the Ni−O−Gd bridging angle and $\beta$ is the dihedral angle between the O−Ni−O and O−Ln−O planes in the bridging fragment.

bridged YNi complex **1a** (all attempts to obtain the YNi complex isostructural to **8** were unsuccessful) extracted from the susceptibility ($D_{Ni}$ = 3.1 $cm^{-1}$ and $g$ = 2.12, see Supporting Information, Figure S4) and magnetization data ($D_{Ni}$ = 2.5 $cm^{-1}$ and $g$ = 2.135) support the magnitude of the $D_{Ni}$ obtained for compound **1**. It is interesting to note that the $J$ values did not significantly change when either $D_{Ni}$ was fixed to zero and/or a term accounting for the intermolecular interactions by means of the molecular field approximation, $-zJ'\langle S_z\rangle S_z$, was introduced in the Hamiltonian (Supporting Information, Table S8). The values of $J_{NiGd}$ for complexes **1** and **8** fall within the range of 0.3−5 $cm^{-1}$ found for alkoxo- and phenoxo-bridged Gd···Ni complexes with ferromagnetic interactions (Table 1).[24−29] It should be noted that the $J_{NiGd}$ values found for complexes bearing three phenoxo bridges connecting $Gd^{III}$ and $Ni^{II}$ (generally formed by tripodal ligands) are lower than those observed for complexes bearing only two of these bridges (generally formed by compartmental ligands), which, among other reasons, should be because in the triply bridged structures each pair of phenoxo bridging fragments $Gd(O)_2Ni$ is folded and consequently exhibits smaller Ni−O−Gd angles than the planar fragments. In line with this, the $J_{NiGd}$ value for **8** is similar to those found for other near-planar diphenoxo-bridged GdNi dinuclear complexes with large Gd−O−Ni angles, which are within the range 2.1−3.6 $cm^{-1}$ (Table 1). The $J_{NiGd}$ value for **1**, with a folded structure and smaller average Ni−O−Gd angle, exhibits, as expected, a rather lower value of the magnetic exchange coupling. Noteworthy, two of these alkoxo- or phenoxo-bridged $Ni_xGd$ complexes ($x$ = 1, 2, 3) exhibit antiferromagnetic interactions.[30,31] By analyzing the structural factors included in Table 1, no rational or obvious explanation can be drawn to justify this behavior: one of the compounds exhibits the lowest $\theta$ and the highest $\beta$ angles, but, conversely, the other has large $\theta$ and small $\beta$ angles.

The field dependencies of the magnetization at 2 K for **1** and **8** (Figure 9) show a relatively rapid increase in the magnetization at low field, in agreement with a high-spin

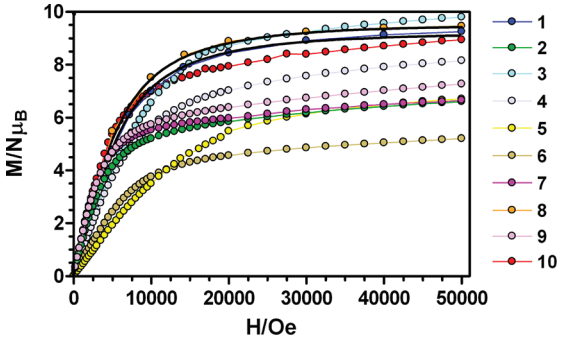


**Figure 9.** $M$ versus $H$ plots for complexes **1**−**10** at 2 K. Black solid lines correspond to Brillouin functions for $S$ = 9/2 with $g$ = 2.04 and 2.10 for **1** and **8**, respectively. The rest of the solid lines are a guide to the eye.

state, and a rapid saturation of the magnetization that is almost complete above 4 T, reaching values of 9.25 $\mu_B$ and 9.46 $\mu_B$, respectively. These are in good agreement with the theoretical value for a $S_T$ = 9/2 spin ground state (9 $\mu_B$ for $g$ = 2). The experimental data for compounds **1** and **8** are well reproduced by the $S$ = 9/2 Brillouin function, indicating the absence of a marked anisotropy, which is also confirmed by the $M$ versus $H/T$ data that are approximately superposed (see Supporting Information, Figure S5). It is interesting to note at this point that the simulated $M$ versus $H$ plot for **1** using $J$ = +1.38 $cm^{-1}$ does not vary when $D_{Ni}$ is varied in the 0−4 $cm^{-1}$ range and therefore the susceptibility and magnetization data are not in conflict. The fitting results seem to indicate that the magnetic exchange coupling is almost insensitive to the ZFS and/or intermolecular interactions operating at very low temperature.

To support the experimental values of the $J_{NiGd}$ for complexes **1** and **8**, DFT calculations were carried out on the X-ray structures as found in the solid state. The calculated $J_{NiGd}$ parameters (+2.05 and +3.3 for **1** and **8**, respectively) agree in sign and rather well in magnitude with the experimental


dx.doi.org/10.1021/ic3004596 | Inorg. Chem. 2012, 51, 5857−5868

parameters (+1.38 and +2.16 for **1** and **8**, respectively). It should be noted that theoretical studies carried out on di-$\mu$-phenoxo dinuclear Gd-$(O)_2$-Cu complexes,[32] and very recently on related Gd-$(O)_2$-Ni complexes,[33] indicated that the ferromagnetic interaction between $M^{II}$ (Cu, Ni) and $Gd^{III}$ ions increases with the planarity of the M−$(O)_2$−Gd fragment and with the increase of the Ni−O−Gd angle. Complexes **1** and **8** are excellent candidates to check these magneto-structural correlations, as they contain the same ligand and show similar structures; almost planar for the former and folded for the latter. The calculated and experimental $J_{NiGd}$ values seem to support the above theoretical correlations as compound **8**, having a larger $\theta$ angle (average value of 109.47°) and a lower $\beta$ angle (2.3° respectively) than **1** (with average $\theta$ and $\beta$ angles of 104. 37° and 21.4°, respectively) exhibits a larger ferromagnetic coupling. Nevertheless, to confirm that the above theoretical magneto-structural correlation also applies in our complexes, we have performed calculations on the simple model compound, $[Ni(PMTA)(H_2O)(\mu\text{-}OPh)_2Gd(OCH_3)_2(NO_3)_3]$ (where PMTA = 1,1,4,7,7-pentamethyldiethylenetriamine and $OPh^-$ = 4-methylphenolato anion; Figure 10), in which, with respect to compound **8**, the part of ligand containing the amino nitrogen atoms have been replaced by 1,1,4,7,7-pentamethyl-diethylenetriamine, the phenoxo-bridging parts of the ligand by 4-methyl-phenolato bridging groups, and the methoxy groups coordinated to the $Gd^{III}$ ion by methanol molecules.

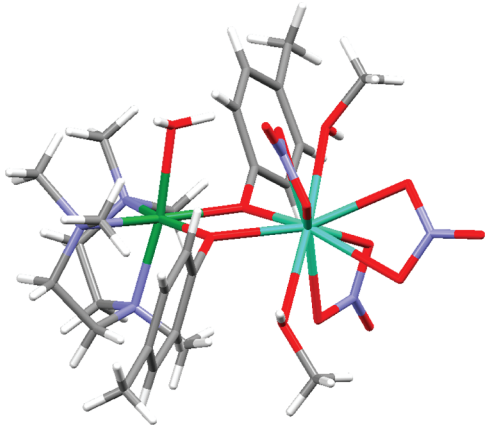

**Figure 10.** $[Ni(PMTA)(H_2O)(\mu\text{-}OPh)_2Gd(OCH_3)_2(NO_3)_3]$ model compound used in DFT calculations. Color code: N = blue, O = red, Ni = green, Dy = light blue, C = gray.

In these calculations, first, the hinge angle, $\beta$, was fixed to zero (planar Ni-$(O)_2$-Gd bridging fragment) and the $\theta$ angle varied in the 90°−115° range. In all cases, the phenyl rings were turned away from the Ni$(O)_2$Gd bridging plane by about 25° to avoid steric hindrance with neighboring parts of the molecule. The DFT results (see Figure 11) clearly show that there exists a linear relationship between $J$ and $\theta$ ($r^2$ = 0.99) and for angles larger than 91° (the crossover point below which the magnetic interaction changes from ferromagnetic to antiferromagnetic) the magnetic exchange interaction is ferromagnetic in nature, and its magnitude increases when $\theta$ increases reaching a value of +3.6 $cm^{-1}$ at 115°. The calculated $J_{NiGd}$ values are of the same order of magnitude but slightly higher than those observed for compound **8**. To know how the folding of the structure affects the $J_{NiGd}$ we have carried out calculations on the model compound for two different values of the $\theta$ angle (110° and 100° that are the ends of the range of $\theta$ angles usually observed in this type of compound) and for each of these values the hinge angle, $\beta$, was varied between 0° and 30° (Figure 11). The results show that, in general, for a fixed $\theta$ value, the $J_{NiGd}$ first decreases on going from 0° to 30°. It should be noted that the aim of these calculations on the model compound $[Ni(PMTA)(H_2O)(\mu\text{-}OPh)_2Gd(OCH_3)_2(NO_3)_3]$ is not to faithfully reproduce the experimental $J_{NiGd}$ values but to know if the theoretical magneto-structural correlation found for the analogous $Ni^{II}$-$Gd^{III}$ dinuclear complex containing a hexadentate di-$\mu$-phenoxo bridging Schiff base ligand, $[L_1Ni(H_2O)_2Gd(NO_3)_3]$ ($L_1$ = [2,2-[2,2-dimethyl-1,3-propanediylbis(nitrilomethylidyne)]bis(6-methoxyphenolato)-(2-)]nickel(II)])[33] (which was obtained using a different approach) is also operative in our compounds. The DFT results point out that although our model compound exhibits a similar trend (the ferromagnetic interaction between $Gd^{III}$ and $Ni^{II}$ ions increases when $\theta$ increases and $\beta$ decreases), there are significant differences between both calculations. First, the calculated $J_{NiGd}$ values for $[L_1Ni(H_2O)_2Gd(NO_3)_3]$ are slightly smaller than those for our model compound and predict the crossover point between ferromagnetic and antiferromagnetic interactions at $\theta$ =84°. Second, the $J_{NiGd}$ values steadily decrease when the $\beta$ angle increase for $[L_1Ni(H_2O)_2Gd(NO_3)_3]$ reaching a value of ∼+0.8 $cm^{-1}$ at 40°, whereas for our model compound, the decrease is much more abrupt, predicting antiferromagnetic interactions for $\beta$ = 30° when $\alpha$ = 100°.

Finally, to disclose how the presence of a third nonphenoxo bridge affects the magnetic exchange coupling between $Gd^{III}$ and $Ni^{II}$, DFT calculations were carried out on a model compound where the *syn-syn* acetate bridging group connecting the $Gd^{III}$ and $Ni^{II}$ ions in **1** was replaced by two nonbridging water molecules, without modifying the remainder of the structure. The results of these calculations show that the $J_{NiGd}$

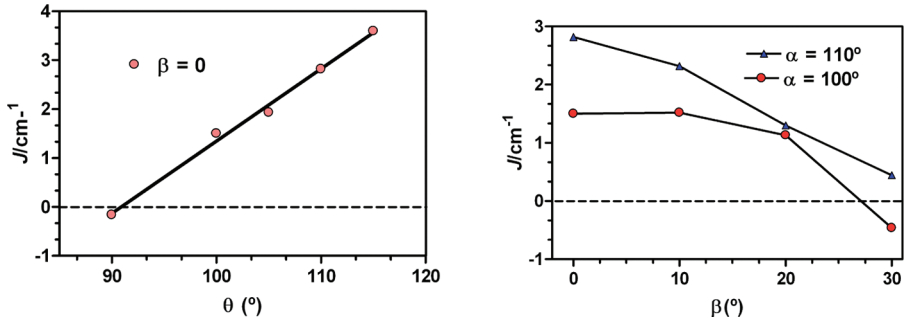


**Figure 11.** $J_{NiGd}$ versus $\theta$ (left) and $J_{NiGd}$ versus $\beta$ (right) plots.


dx.doi.org/10.1021/ic3004596 | *Inorg. Chem.* 2012, 51, 5857−5868

value increases from +2.05 $cm^{-1}$ in **1** to +2.5 $cm^{-1}$ for the model compound. This result clearly underlines that, in addition to the hinge angle, the third bridge has a significant role in decreasing the magnetic exchange coupling in this type of compound with respect to the analogous planar diphenoxo-bridged GdNi complexes bearing similar to $H_2L$ binucleating Schiff base derivative ligands.

We now discuss the magnetic properties of complexes **2**−**7**, **9**, and **10**. At room temperature, the $\chi_M T$ products of these complexes are very close to the calculated values for independent $Ni^{II}$ ($S$ = 1 with $g_{Ni}$ = 2.0) and/or $Ln^{III}$ ions in the free-ion approximation (see Supporting Information, Table S9). The $\chi_M T$ values for **2**, **9**, and **10** decreases slowly with decreasing temperature, reaching a minimum in the 20−25 K temperature range (Supporting Information, Table S9). This behavior is due to depopulation of the Stark sublevels of the $Ln^{III}$ ion, which arise from the splitting of the ground term by the ligand field and whose width is of the order of 100 $cm^{-1}$.[34] Below the temperature of the minimum, $\chi_M T$ increases to reach a maximum at 4 K and then shows a sharp decrease down to 2 K. The increase in $\chi_M T$ below ∼25 K is due to a ferromagnetic interaction between $Ni^{II}$ and $Ln^{III}$, whereas the decrease of $\chi_M T$ below 4 K is likely associated with the presence of magnetic anisotropy and/or weak antiferromagnetic interactions between the dinuclear complexes. At variance, the $\chi_M T$ for **7** steadily increases with decreasing temperature to reach a maximum at 4 K and then drops abruptly down to 2 K. The increase in the $\chi_M T$ product **7** indicates, on the one hand, that the effect of depopulation of the Stark sublevels is not as pronounced as in **2** and, on the other hand, the existence of a ferromagnetic exchange interaction between the $Ni^{II}$ and $Tb^{III}$ ions.

The $\chi_M T$ products for **3** and **4** decrease with decreasing temperature, first slightly until around 50 K and then sharply to 2 K. This behavior is mainly due to the depopulation of the Stark sublevels of the $Ho^{III}$ and $Er^{III}$ ions. To know the nature of the magnetic interaction between $Ni^{II}$ and either $Ho^{III}$ and $Er^{III}$ ions, we adopted a previously reported empirical approach,[35] in which the contribution of the crystal-field effects of the $Ln^{III}$ ion is removed by subtracting from the experimental $\chi_M T$ data of **3** and **4** those of the isostructural complexes **5** and **6**, respectively, whose magnetic behavior depends only on the $Ln^{III}$ ion. The difference $\Delta\chi_M T = (\chi_M T)_{NiLn} - (\chi_M T)_{ZnLn}$ is therefore related to the nature of the overall exchange interaction between the $Ni^{II}$ and $Ln^{III}$ ions. Thus, positive values are related to ferromagnetic couplings whereas negative values are related to antiferromagnetic interactions. The $\Delta\chi_M T$ values are almost constant over the whole temperature range (see Figure 12), except for an increase in the lowest-temperature region, thus indicating a ferromagnetic interaction between $Ni^{II}$ and $Ln^{III}$ ions. It seems that the magnetic exchange coupling is higher for **3** than for **4** as the $\Delta\chi_M T$ values for the former begin to increase at higher temperatures.

The field dependence of the magnetization at 2 K for compounds **2**−**7**, **9**, and **10** are shown in Figure 9. The $M$ versus $H$ plots for compound **2**−**4**, **7**, **9**, and **10** show a relatively rapid increase of the magnetization at low field, in accord with the ferromagnetic interaction between $Ni^{II}$ and $Ln^{III}$, and a linear increase at high field without achieving a complete saturation at 5 T. This behavior suggests the presence of a significant magnetic anisotropy and/or more likely the presence of low-lying excited states that are partially (thermally and field-induced) populated. These low-lying excited states are in agreement with weak magnetic interactions expected for 3d-4f systems. The magnetization values for **2**−**4**, **7**, **9**, and **10** at 5 T are considerably smaller than the expected saturation magnetization value, $Ms/N\mu_B = g_J J$, for a $Ln^{III}$ ion that has a strong easy-axis anisotropy, and behaves as an Ising spin at low temperatures with the maximum absolute $J_z$ value, ferromagnetically coupled with the $S$ = 1 value for the $Ni^{II}$ ion (see Supporting Information, Table S9). This behavior could be due to the existence of sublevels having absolute $J_z$ values lower than the maximum absolute $J_z$ value as the most stable, leading to a $Ln^{III}$ ion that does not yet have easy-axis anisotropic character, and/or to the misalignment between the principal axis of the microcrystals and the magnetic field.

The magnetization at low field for compound **7** increases more rapidly than that for compound **2**, which could be due to the expected stronger magnetic exchange coupling for the former as it has a smaller hinge angle (13.73° vs 22.32°) and almost equal average Ni−O−Tb bridging angle (104.73° vs 104.28°). In fact, DFT calculations on the hypothetical complex $[Ni(\mu\text{-}L)(\mu\text{-}NO_3)Gd(NO_3)_2]$, which was built from **7** replacing $Tb^{III}$ by $Gd^{III}$, lead to a $J_{NiGd}$ value of +2.26 $cm^{-1}$ slightly larger than that calculated for compound **1** (isostructural to **2**) of +2.05 $cm^{-1}$.

The $M$ versus $H$ plots for **3** and **4** (Figure 12) exhibit a rapid increase of the magnetization compared to complexes **5** and **6**,

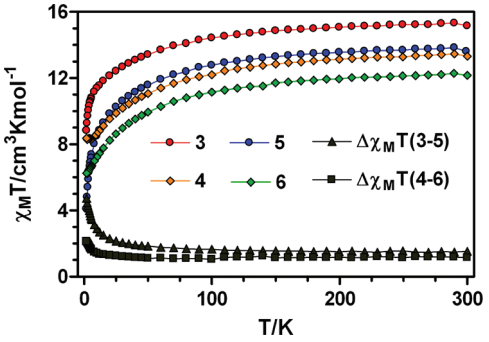


**Figure 12.** Temperature dependence of the $\chi_M T$ product for **3**−**6** and the differences $\Delta\chi_M T = (\chi_M T)_{NiTb} - (\chi_M T)_{ZnTb}$.

which supports the ferromagnetic interaction between $Ni^{II}$ and $Ln^{III}$ in these complexes. The $M$ value for **9** at 5 T is lower than that of **10** (see Supporting Information, Table S9), which might indicate a weaker anisotropy for the latter compound. The differences in the $Dy^{III}$ coordination sphere and therefore in the ligand field surrounding the lanthanide ion indicated elsewhere, which are mainly caused by the coordination of a bidentate 9-anthracenecarboxylate ligand instead of a bidentate nitrate ligand, may be responsible for the different anisotropies exhibited by complexes **9** and **10**.

Dynamic alternating current (ac) magnetic susceptibility measurements as a function of the temperature at different frequencies were performed on these complexes under zero-external field, but only complexes **9** and **10** show a frequency dependency of the in-phase ($\chi'_M$) and out-of-phase ($\chi''_M$) signals (Supporting Information, Figure S6). This behavior indicates slow relaxation of the magnetization typical of a SMM. However, none exhibit any maximum in the temperature dependence of $\chi''_M$ above 2 K at frequencies reaching 1400 Hz. This feature could be due to the existence of fast quantum tunneling relaxation of the magnetization. When the ac measurements were performed in the presence of a small external direct current (dc) field of 1000 G to fully or partly


dx.doi.org/10.1021/ic3004596 | Inorg. Chem. 2012, 51, 5857−5868

suppress the quantum tunneling relaxation, compound **7** showed slow relaxation of the magnetization without a clear maximum above 2 K, whereas complexes **9** and **10** exhibited typical SMM behavior below 5 K with maxima in the 2.25 K (619 Hz)−2.75 K (1399 Hz) and 2 K (300 Hz)−3 K (1400 Hz) ranges for **9** and **10**, respectively (Figures 13 and 14).

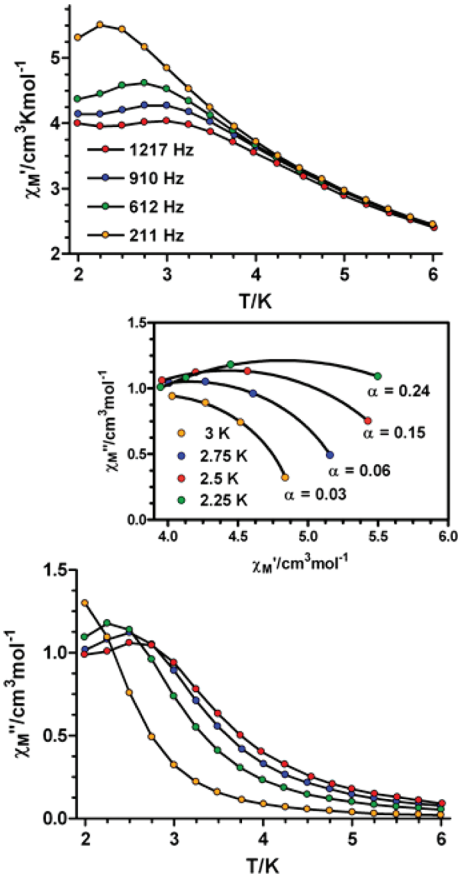


**Figure 13.** Temperature dependence of in-phase $\chi'_M$ (top) and out-of-phase $\chi''_M$ (bottom) components of the ac susceptibility for complex **9** measured under 1000 Oe applied dc field. Bottom inset: Cole−Cole (Argand) plot of $\chi'_M$ versus $\chi''_M$ in the 2.25−3.0 K temperature range, in 1000 Oe applied dc field, for compound **9**. The solid lines represent the best fit of the data to a generalized Debye model.

The Cole−Cole plots in the temperature range 2.25−3 K for **9** and 2.4−3.4 K for **10** exhibit semicircular shapes with $\alpha$ parameters in the ranges 0.03−0.24 and 0.07−0.20, respectively, suggesting multiple relaxation processes. From the temperatures and frequencies of the maxima observed for the $\chi''_M$ signals, and by using an Arrhenius plot, $\tau = \tau_0 \exp(\Delta/k_BT)$, the thermally activated energy barriers for the flipping of the magnetization ($\Delta/k_B$) were estimated to be 9.2 and 10.1 K for **9** and **10**, respectively, and the flipping rates $\tau_0$ were $4.4 \times 10^{-6}$ s and $3.4 \times 10^{-6}$ s. The values of $\Delta/k_B$ are at the lower end of the experimental range found for similar 3d/4f SMM systems,[6−9] but the $\tau_0$ values are much larger than expected. These data suggest that the applied field of 1000 G is unable to fully suppress the quantum pathway of the relaxation in **9** and **10** and therefore their thermal energy barriers should actually be higher than the above estimated values. As **10** is characterized by a $\Delta/k_B$ slightly higher and a $\tau_0$ slightly lower than those found for **9**, the out-of-phase signals for the former appear at slightly higher temperatures. This would be in

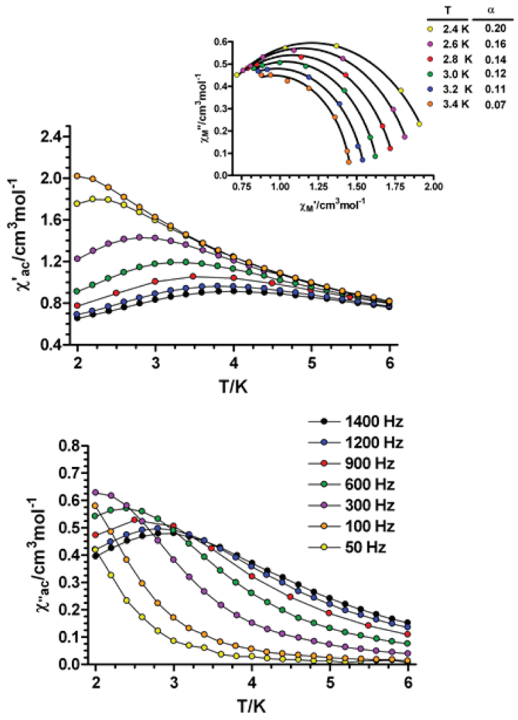


**Figure 14.** Temperature dependence of in-phase $\chi'_M$ (top) and out-of-phase $\chi''_M$ (bottom) components of the ac susceptibility for complex **10** measured under 1000 Oe applied dc field. Top inset: Cole−Cole (Argand) plot of $\chi'_M$ versus $\chi''_M$ in the 2.4−3.04 K temperature range, in 1000 Oe applied dc field, for compound **10**. The solid lines represent the best fit of the data to a generalized Debye model.

agreement with the higher easy-axis anisotropy suggested for **10** from dc data.

## CONCLUDING REMARKS

The use of a specifically designed compartmental Mannich type ligand *N,N′,N″*-trimethyl-*N,N″*-bis(2-hydroxy-3-methoxy-5-methylbenzyl)diethylenetriamine ($H_2L$), containing $N_3O_2$ and $O_4$ inner and outer pockets, respectively, allows the synthesis, in one pot reaction, of some examples of nitrate-diphenoxo and acetate-diphenoxo triply bridged dinuclear complexes $[M(\mu\text{-}L)(\mu\text{-}X)Ln(NO_3)_2]$ (X = $OAc^-$ and $NO_3^-$, $M^{II}$ = $Ni^{II}$, $Zn^{II}$ and $Ln^{III}$ = Eu, Gd, Tb, Ho, Er, and Y; $M^{II}$ = $Zn^{II}$), as well as two examples of diphenoxo doubly bridged complexes $[Ni(H_2O)(\mu\text{-}L)Ln(NO_3)_3]\cdot 2CH_3OH$ ($Ln^{III}$ = Eu, Gd). $Ni^{II}$−$Dy^{III}$ dinuclear complexes can be used as platform to obtain other carboxylatediphenoxo-bridged complexes such as $[Ni(\mu\text{-}L)(\mu\text{-}BzO)Dy(NO_3)_2]$ and $[Ni(\mu\text{-}L)(\mu\text{-}9\text{-}An)Dy(9\text{-}An)(NO_3)_2]\cdot 3CH_3CN$. The former contains a benzoate-bridging group connecting $Ni^{II}$ and $Dy^{III}$ metal ions whereas the latter has both bridging and chelating 9-An ligands. Triply bridged complexes exhibit folded structures with rather asymmetrical M−$(O)_2$−Gd bridging fragments, whereas diphenoxo-bridged complexes display almost planar structures and symmetrical bridging fragments. The size of the $Ln^{III}$ ions seems to play a pivotal role in the adoption of a triply or doubly bridged structure in nitrate containing complexes. Thus, metal ions smaller in size than $Gd^{3+}$ always lead to nitratediphenoxo triply bridged dinuclear complexes. Magnetic exchange interactions between $Ni^{II}$ and $Ln^{III}$ metal ions are in all cases ferromagnetic in nature. For $Ni^{II}$-$Gd^{III}$ we have shown from experimental results and DFT calculations that the $J_{NiGd}$ coupling increases


dx.doi.org/10.1021/ic3004596 | Inorg. Chem. 2012, 51, 5857−5868

when the planarity of the M−$(O)_2$−Gd bridging fragment and the Ni−O−Gd bridging angle increase. The $Ni^{II}Dy^{III}$ complexes [Ni($\mu$-L)($\mu$-BzO)Dy$(NO_3)_2$] (**9**) and [Ni($\mu$-L)($\mu$-9-An)Dy(9-An)$(NO_3)_2$]·3$CH_3CN$ (**10**) exhibit slow relaxation of the magnetization with $\Delta/k_B$ energy barriers under 1000 Oe applied magnetic fields of 9.2 and 10.1 K, respectively. Direct current data suggest that the latter compound has higher easy-axis anisotropy than the former complex, and this may be the reason why a larger thermal energy barrier is observed for **10**.

## ■ ASSOCIATED CONTENT

### Supporting Information

Crystallographic data in CIF format, Figures S1−S6 and Table S1−S9. This material is available free of charge via the Internet at http://pubs.acs.org.

## ■ AUTHOR INFORMATION


### Corresponding Author

*E-mail: ecolacio@ugr.es (E.C.), ebrechin@staffmail.ed.ac.uk (E.K.B.).


### Notes

The authors declare no competing financial interest.

## ■ ACKNOWLEDGMENTS


This work was supported by the MEC (Spain) (Project CTQ-2008-02269/BQU and CTQ2011-24478), the Junta de Andalucía (FQM-195 and Projects of excellence P08-FQM-03705 and P11-FQM-7756), and the University of Granada. Financial support from the University of Granada (CEI campus de Excelencia) and Junta de Andalucia for the visit of E.C. to the University of Edinburgh is grateful acknowledged. E.K.B. would like to thank the EPSRC and Leverhulme Trust for financial support. We would like to thank the Centro de Supercomputación de la Universidad de Granada for computational resources.


## ■ REFERENCES


(1) For some recent reviews see: (a) Winpenny, R. E. P. *Chem. Soc. Rev.* **1998**, *27*, 447. (b) Sakamoto, M.; Manseki, K.; Okawa, H. *Coord. Chem. Rev.* **2001**, *219*, 279. (c) Benelli., C.; Gatteschi, D. *Chem. Rev.* **2002**, *102*, 2369. (d) Sessoli, R.; Powell, A. K. *Coord. Chem. Rev.* **2009**, *253*, 2328. (e) Andruh, M.; Costes, J. P.; Diaz, C.; Gao, S. *Inorg. Chem.* **2009**, *48*, 3342 (Forum Article). (f) Andruh, M. *Chem. Commun.* **2011**, *47*, 3015. (g) Sorace, L.; Benelli, C.; Gatteschi, D. *Chem. Soc. Rev.* **2011**, *40*, 3092.

(2) For some recent reviews see: (a) Gatteschi, D.; Sessoli, R. *Angew. Chem., Int. Ed.* **2003**, *42*, 268. (b) Christou, G. *Polyhedron* **2005**, *24*, 2065. (c) Gatteschi, D.; Sessoli, R.; Villain, J. *Molecular Nanomagnets*; Oxford University Press: Oxford, U.K., 2006. (d) Aromí, G.; Brechin, E. K. *Struct. Bonding (Berlin)* **2006**, *122*, 1. (e) Rebilly, J.-N.; Mallah, T. *Struct. Bonding (Berlin)* **2006**, *122*, 103. (f) Cornia, A.; Costantino, A. F.; Zobbi, L.; Caneschi, A.; Gatteschi, D.; Mannini, M.; Sessoli, R. *Struct. Bonding (Berlin)* **2006**, *122*, 133. (g) Milios, C. J.; Piligkos, S.; Brechin, E. K. *Dalton Trans* **2008**, 1809. (h) "Molecular Magnets", themed issue (Brechin, E. K., Ed.), *Dalton Trans.*, 2010, (i) Bagai, R.; Christou, G. *Chem. Soc. Rev.* **2009**, *38*, 1011. (j) Glaser, T. *Chem. Commun.* **2011**, *47*, 116.

(3) (a) Wernsdorfer., W.; Sessoli, R. *Science* **1999**, *284*, 133. (b) Leuenberger, M. N.; Loss, D. *Nature* **2001**, *410*, 789. (c) Meier, F.; Loss, D. *Phys. B* **2003**, *329*, 1140. (d) Bogani, L.; Wernsdorfer, W. *Nat. Mater.* **2008**, *7*, 179.

(4) Zadrozny, J. M.; Liu, J.; Piro, N. A.; Chang, C. J.; Hill, S.; Long, J. R. *Chem. Commun.* **2012**, DOI: 10.1039/C2CC16430B, and references therein.

(5) Kajiwara, T.; Nakano, M.; Takahashi, K.; Takaishi, S.; Yamashita, M. *Chem.—Eur. J.* **2011**, *17*, 196 , and references therein.

(6) See for instance: (a) Iasco, O.; Novitchi, G.; Jeanneau, E.; Wernsdorfer, W.; Luneau, D. *Inorg. Chem.* **2011**, *50*, 7373. (b) Papatriantafyllopoulou, C.; Wernsdorfer, W.; Abboud, K. A.; Christou, G. *Inorg. Chem.* **2011**, *50*, 421. (c) Mondal, K. C.; Kostakis, G. E.; Lan, Y.; Wernsdorfer, W.; Anson, C. E.; Powell, A. K. *Inorg. Chem.* **2011**, *50*, 11604. (d) Zou, L.-F.; Zhao, L.; Guo, Y.-N.; G.-Miao, Y.; Guo, Y.; Tang, J.; Li, Y.-H. *Chem. Commun.* **2011**, *47*, 8569. (e) Rinck, J.; Novitchi, G.; Heuvel, W. V. d.; Ungur, L.; Lan, Y.; Wernsdorfer, W.; Anson, C. E.; Chibotaru, L. F.; Powell, A. K. *Angew.Chem., Int. Ed.* **2010**, *49*, 7583. (f) Yamaguchi, T.; Costes, J. P.; Kishima, Y.; Kojima, M.; Sunatsuki, Y.; Brefuel, N.; Tuchagues, J. P.; Vendier, L.; Wernsdorfer, W. *Inorg. Chem.* **2010**, *49*, 9125. (g) Schray, D.; Abbas, G.; Lan, Y.; Mereacre, V.; Sundt, A.; Dreiser, J.; Waldmann, O.; Kostakis, G. E.; Anson, C. E.; Powell, A. K. *Angew. Chem., Int. Ed.* **2010**, *49*, 5185.

(7) (a) Kajiwara, T.; Nakano, M.; Takaishi, S.; Yamashita, M. *Inorg. Chem.* **2008**, *47*, 8604. (b) Kajiwara, T.; Takahashi, K.; Hiraizumi, T.; Takaishi, S.; Yamashita, M. *CrystEngComm* **2009**, *11*, 2110. (c) Kajiwara, T.; Takahashi, K.; Hiraizumi, T.; Takaishi, S.; Yamashita, M. *Polyhedron* **2009**, *28*, 1860.

(8) (a) Costes, J.-P.; Dahan, F.; Dupuis, A.; Laurent, J. P. *Inorg Chem* . **1997**, *36*, 3429.

(9) (a) Costes, J.-P.; Dupuis, A.; Laurent, J. P. *J. Chem. Soc., Dalton Trans.* **1998**, 735. (b) Costes, J.-P.; Dupuis, A.; Laurent, J. P. *Eur. J. Inorg. Chem.* **1998**, 1543. (c) Costes, J.-P.; Dahan, F.; Donnadieu, B.; Garcia-Tojal, J.; Laurent, J. P. *Eur. J. Inorg. Chem.* **2001**, 363. (d) Costes, J. P.; Clemente-Juan, J. M.; Dahan, F.; Dumestre, F.; Tuchagues, J. P. *Inorg. Chem.* **2002**, *41*, 2886. (e) Costes, J. P.; Dahan, F.; Dupuis, A.; Laurent, J. P. *C. R. Acad. Sci .Paris, IIc* **1998**, 417. (f) Costes, J. P.; Dahan, F.; Garcia Tojal, J. *Chem.—Eur. J.* **2002**, *8*, 5430. (g) Gómez, V.; Vendier, L.; Corbella, M.; Costes, J.-P. *Eur. J. Inorg. Chem.* **2011**, *17*, 2653. (h) Costes, J.-P.; Dahan, F.; Dupuis, A.; Laurent, J. P. *Inorg. Chem.* **1997**, *36*, 4284. (i) Mori, F.; Ishida, T.; Nogami., T. *Polyhedron* **2005**, *24*, 2588. (j) Chen, Q.-Y.; Luo, Q.-H.; Zheng, L.-M.; Wang, Z.-L.; Chen, J.-T. *Inorg. Chem.* **2002**, *41*, 605. (k) Costes, J. P.; Vendier, L. *Eur. J. Inorg. Chem.* **2010**, 2768. (l) Yamaguchi, T.; Sunatsuki, Y.; Ishida, H.; Kojima, M.; Akashi, H.; Re, N.; Matsumoto, N.; Pochaba, A.; Mrozinski, J. *Inorg. Chem.* **2008**, *47*, 5736. (m) Colacio, E.; Ruiz-Sanchez, J.; White, F. J.; Brechin, E. K. *Inorg. Chem.* **2011**, *50*, 7268. (n) Pasatoiu, T. D.; Sutter, J.-P.; Madalan, A. M.; Fellah, F. Z. C.; Duhayon, C.; Andruh, M. *Inorg. Chem.* **2011**, *50*, 5890.

(10) (a) Lisowski, J.; Starynowicz, P. *Inorg. Chem.* **1999**, *38*, 1351. (b) Sanada, T.; Suzuki, T.; Kaizaki, S. *J. Chem. Soc., Dalton Trans.* **1998**, 959.

(11) *Supernova CCD system, CrysAlisPro Software system*, Version 1.171.33.55; Oxford Diffraction Ltd.: Abindon. U.K., 2007.

(12) Sheldrick, G. M. *Acta Crystallogr., Sect. A* **2008**, 64112.

(13) Soler, J. M.; Artacho, E.; Gale, J. D.; Garcia, A.; Junquera, J.; Ordejon, P.; Sanchez-Portal, D. *J. Phys.: Condens. Matter* **2002**, *14*, 2745.

(14) Perdew, J. P.; Burke, K.; Ernzerhof, M. *Phys. Rev. Lett.* **1996**, *77*, 3865.

(15) Kleinman, L.; Bylander, D. M. *Phys. Rev. Lett.* **1982**, *48*, 1425.

(16) Troullier, N.; Martins, N. J. L. *Phys. Rev. B* **1991**, *43*, 1993.

(17) Pollet, R.; Marx, D. *J. Chem. Phys.* **2007**, *126*, 181102.

(18) Ruiz, E.; Alvarez, S.; Cano, J.; Polo, V. *J. Chem. Phys.* **2005**, *123*, 164110.

(19) Ruiz, V.; Rodríguez-Fortea, A.; Tercero, J.; Cauchy, T.; Massobrio, C. *J. Chem. Phys.* **2005**, *123*, 74102.

(20) Ruiz, E.; Alemany, P.; Alvarez, S.; Cano, J. *J. Am. Chem. Soc.* **1997**, *119*, 1297.

(21) Figgis, B. N.; Hitchman, M. A. *Ligand Field Theory and its applications*; Wiley-VCH: New York, 2000.

(22) Nolet, M.-C.; Michaud, A.; Bain, C.; Zargarian, D.; Reber, C. *Photochem. Photobiol.* **2006**, *82*, 57.

(23) Llunell, M.; Casanova, D.; Cirera, J.; Bofill, J. M.; Alemany, P.; Alvarez, S.; Pinsky, M.; Avnir, D. *SHAPE*, v1.1b; Barcelona, Spain, 2005.
(24) MAGPACK program. Borrás-Almenar, J. J.; Clemente-Juan, J. M.; Coronado, E.; Tsukerbalt, B. S. *J. Comput. Chem.* **2001**, *22*, 985.
(25) Shiga, T.; Ito, N.; Hidaka, A.; Ohkawa, H.; Kitagawa, S.; Ohba, M. *Inorg. Chem.* **2007**, *46*, 3492.
(26) Costes, J.-P.; Yamaguchi, T.; Kojima, M.; Vendier, L. *Inorg. Chem.* **2009**, *48*, 5555.
(27) Georgopoulou, A. N.; Efthymiou, C. G.; Papatriantafyllopoulou, C.; Psycharis, V.; Raptopoulou, C. P.; Manos, M.; Tasiopoulos, A. J.; Escuer, A.; Perlepes, S. P. *Polyhedron* **2011**, *30*, 2978.
(28) Costes, J. P.; Yamaguchi, T.; Kojima, M.; Vendier, L. *Inorg. Chem.* **2009**, *48*, 5555.
(29) Chandrasekhar, V.; Pandian, B. M.; Boomishankar, R.; Steiner, A.; Vittal, J. J.; Houri, A.; Clérac, R. *Inorg. Chem.* **2008**, *47*, 4918.
(30) Efthymiou, C. G.; Stamatatos, T. C.; Papatriantafyllopoulou, C.; Tasiopoulos, A. J.; Wernsdorfer, W.; Perlepes, S. P.; Christou, G. *Inorg. Chem.* **2010**, *49*, 9737.
(31) Georgopoulou, A. N.; Adam, V.; Raptopoulou, C. P.; Psycharis, V.; Ballesteros, R.; Abarca, B.; Boudalis, A. K. *Dalton Trans.* **2010**, *39*, 5020.
(32) (a) Cirera, J.; Ruiz, E. *C. R. Chim.* **2008**, *11*, 1227. (b) Costes, J. P.; Dahan, F.; A. Dupuis, A. *Inorg. Chem.* **2000**, *39*, 165. (c) Rajaraman, G.; Totti, F.; Bencini, A.; Caneschi, A.; Sessoli, R.; Gatteschi, D. *Dalton Trans.* **2009**, 3153.
(33) Singh, S. K.; Tibrewal, N. K.; Rajaraman, G. *Dalton Trans.* **2011**, *40*, 10897.
(34) (a) Benelli, C.; Gatteschi, D. *Chem. Rev.* **2002**, *102*, 2369 , and references therein. (b) Sutter, J. P.; Kahn, O. *Magnetism: Molecules to Materials*; Miller, J. S., Drillon, M., Eds.; Wiley-VCH: Weinheim, Germany, 2005; p 161.
(35) See for instance: (a) Costes, J.-P.; Dahan, F.; Dupuis, A.; Laurent, J.-P. *Chem.—Eur. J.* **1998**, *4*, 1616. (b) Kahn, M. L.; Mathoniere, C.; Kahn, O. *Inorg. Chem.* **1999**, *38*, 3692.